APPLICATION OF GREEN'S FUNCTIONS IN ANALYSIS OF THE RESPONSE OF AN INFINITE HOMOGENOUS STRUCTURE TO MOVING LOAD

Traian MAZILU[1]

Scopul acestui articol este de a prezenta o metodă numerică bazată pe funcţiile Green pentru a calcula răspunsul unei structuri infinite omogene cauzat de o forţă în mişcare. Structura are două grinzi rezemate continuu pe straturi elastice şi reprezintă modelul obişnuit al căii ferate pe plăci de beton. Este dovedită marea precizie a metodei. Este analizat răspunsul structurii la forţe armonice cu suport fix şi cu suport mobil atât în domeniul frecvenţei, cât şi în domeniul timp.

The aim of this paper is to present a numerical method based on the Green's functions to calculate the response of an infinite homogenous structure to moving load. The structure has two beams continuously supported by elastic layers and represents the common model of the slab track. The high accuracy of the method is proved. The structure response due to stationary and moving harmonic loads is analyzed for both frequency and time domains.

Keywords: Green's functions, Fourier transform, slab track PDE
Classif: 35C15, 35Q72, 65M99

1. Introduction

The present paper deals with the response of an infinite homogeneous structure consisting of two beams continuously supported by elastic layers to moving load. Such a structure represents a common model for the slab track that has been employed in the study of the interaction between a moving vehicle and the slab track [1]. In addition, similar models were used to calculate the slab track response to a moving load [2, 3]. The upper beam describes a rail, the lower one models the slab, while the two elastic layers reflect the properties of the rail pad and the track subsoil.

The railway track structure can be modeled by two kind of mechanical models: the continuous models and the periodical models with discrete supports [4, 5]. One of the oldest models for the railway track, known as a beam on elastic foundation, in fact, a continuous model, was presented by Winkler in 1867 [6].

[1] Reader, Depart. of Railway Vehicles, Faculty of Transports, University POLITEHNICA of Bucharest, Romania, e-mail: traianmazilu@yahoo.com

The continuous models are used for the slab track, but under some conditions, this type of model is proper for the ballasted track as well [7, 8].

In order to solve the equations of the motion for continuous models, many methods have been proposed. For instance, the direct method, the Fourier transformation method and the coupling in the wave-number frequency-domain method are presented by Hussein and Hunt [2] for the case of the non-moving oscillating load. In addition, they have applied the double Fourier transform from the space-time domain to the wave number-frequency domain for the track subject to a moving oscillating load. On the other hand, Wu and Thompson [7, 8] have developed many equivalent multiple degree of freedom (MDOF) models for the track dynamics having as a starting point the receptance of the rail calculated for a unit stationary harmonic load.

In this paper, starting from previous author's researches [9, 10], the Green's functions method is developed to study the response of the slab track due to the moving load. To this end, a numerical approach to obtain the Green's functions of the structure is presented. In order to verify the accuracy of the method, the results from the analytical and numerical method are compared considering the steady-state behaviour of the structure under moving harmonic load. We should have to underline that the Green's functions of the structure are able to simulate the wheel/rail interaction taking into account the nonlinearities of the contact [11].

2. Governing equations

The structure of the slab track is composed of a massive concrete slab, into which the rails are embedded by means of Corkelast. Assuming that the two rails are symmetrically loaded, only half-track is required for modelling (fig. 1).

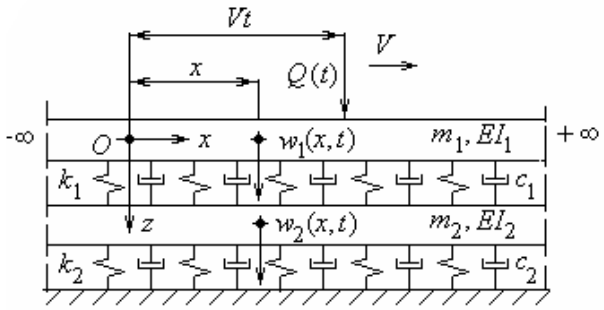

Figure 1. Mechanical model: 1. rail; 2. rail pad; 3. slab; 4. elastic foundation.

In fact, the slab track model may be reduced to a structure consisting of two Euler-Bernoulli beams coupled by Winkler foundation as the rail and the slab and the rail-pad, respectively. The track is supported by the ground that is taken as

a Winkler foundation as well. One has to emphasize that the Euler-Bernoulli beams model gives satisfactory results as long as the cross-sectional dimensions are small compared to the bending wavelength [12] and this hypothesis is considered in the following lines.

The parameters for the track model are: the mass per length unit $m_{1,2}$ (the index 1 for the upper beam and the index 2 for the under beam) and the bending stiffness $EI_{1,2}$. The two Winkler foundations have the elastic constants $k_{1,2}$ per length unit and the viscous damping factors $c_{1,2}$ per length unit.

It is assumed that the track is subjected to a moving load $Q(t)$ depending on the time t, which moves at a constant speed V.

To describe the track evolution under the moving load, the absolutely integrable $\mathbf{C}^4$ functions $w_{1,2}(x,t)$ termed the rail and slab displacement are introduced so that

$$w_{1,2} : \mathbf{R}^2 \to \mathbf{R}\ ,\ w_{1,2}(x,t<0)=0\ , \tag{1}$$

where x is the coordinate along the track. The latest condition refers to the character of the causality. Next, the two functions $w_{1,2}(x,t)$ are encapsulated in the column vector $\mathbf{w}(x,t)=[w_1(x,t)\ \ w_2(x,t)]^{\mathrm{T}}$ termed the column vector of the displacements.

According to the Newton's second law, the column vector $\mathbf{w}(x,t)$ verifies the PDE

$$\mathbf{L}_{x,t}\mathbf{w}(x,t)=\mathbf{q}(x,t) \tag{2}$$

with the boundary and initial conditions

$$\lim_{|x-Vt|\to\infty}\mathbf{w}(x,t)=\left[0\ 0\right]^T\ ,\ \mathbf{w}(x,0)=\left[0\ 0\right]^T\ . \tag{3}$$

where $\mathbf{L}_{x,t}$ stands for the matrix differential operator

$$\mathbf{L}_{x,t}=\begin{bmatrix} D_{EB1}+c_1\dfrac{\partial}{\partial t}+k_1 & -c_1\dfrac{\partial}{\partial t}-k_1 \\ -c_1\dfrac{\partial}{\partial t}-k_1 & D_{EB2}+(c_1+c_2)\dfrac{\partial}{\partial t}+(k_1+k_2) \end{bmatrix}$$

that includes the differential operator of the Euler-Bernoulli beams,

$$D_{EB1,2}=EI_{1,2}\frac{\partial^4}{\partial x^4}+m_{1,2}\frac{\partial^2}{\partial t^2}\ ,$$

and $\mathbf{q}(x,\ t)=[Q(t)\delta(x\text{-}Vt)\ 0]^{\mathrm{T}}$ is the column vector of the forces on the track with $\delta(.)$ the Dirac's delta function.

Theoreme 1. *The boundary value problem formed by the equation (2) and the associated initial conditions (3) has the solution*

$$\mathbf{w}(x,t)=\int_0^t\mathbf{g}(x,Vt',t-t')Q(t')\mathrm{d}t'\ , \tag{4}$$

where the column vector $\mathbf{g}(x,x',t\text{-}t')=[g_1(x,x',t\text{-}t')\ g_2(x,x',t\text{-}t')]^{\mathrm{T}}$ *verifies the equation*

$$\mathbf{L}_{x,t}\mathbf{g}(x,x',t-t') = \delta(x-x')\delta(t-t')[1\ 0]^{\mathrm{T}}. \tag{5}$$

Proof. In order to solve the equation (2), one can apply the 2D Fourier transform with respect to time and spatial coordinate:

$$\mathbf{L}_{\xi,\omega}\mathbf{W}(\xi,\omega) = \mathbf{Q}(\xi,\omega), \tag{6}$$

where

$$\mathbf{W}(\xi,\omega) = \int_{-\infty}^{\infty}\int_{-\infty}^{\infty}\mathbf{w}(x,t)\exp[-\mathrm{i}(\omega t+\xi x)]\mathrm{d}x\mathrm{d}t,$$

$$\mathbf{Q}(\xi,\omega) = \int_{-\infty}^{\infty}\int_{-\infty}^{\infty}\mathbf{q}(x,t)\exp[-\mathrm{i}(\omega t+\xi x)]\mathrm{d}x\mathrm{d}t,$$

(where the integrals with respect to t verify $\int_{-\infty}^{\infty} = \int_{0}^{\infty}$) and

$$\mathbf{L}_{\xi,\omega} = \begin{bmatrix} EI_1\xi^4 - \omega^2 m_1 + k_1 + \mathrm{i}\omega c_1 & -k_1 - \mathrm{i}\omega c_1 \\ -k_1 - \mathrm{i}\omega c_1 & EI_2\xi^4 - \omega^2 m_1 + k_1 + k_2 + \mathrm{i}\omega(c_1+c_2) \end{bmatrix}$$

is the 2D Fourier transform with respect to time and spatial coordinate of the matrix operator $\mathbf{L}_{x,t}$, ξ is the coordinate of the wave-number-domain, ω is the coordinate of the frequency-domain and $\mathrm{i}^2 = -1$. The components of the matrix $\mathbf{L}_{\xi,\omega}$ are in $\mathbf{C}[\xi,\omega]$.

From Eq. (6) one reads

$$\mathbf{W}(\xi,\omega) = \mathbf{L}^{-1}_{\xi,\omega}\mathbf{Q}(\xi,\omega), \tag{7}$$

where the components of the inverse matrix $\mathbf{L}^{-1}_{\xi,\omega}$ are in $\mathbf{C}(\xi,\omega)$.

Let the matrix $\mathbf{\Gamma}(x,t) \in \mathbf{M}_{2\times 2}$ so that

$$\mathbf{\Gamma}(x,t) = \frac{1}{4\pi^2}\int_{-\infty}^{\infty}\int_{-\infty}^{\infty}\mathbf{L}^{-1}_{\xi,\omega}\exp[\mathrm{i}(\omega t+\xi x)]\mathrm{d}\omega\mathrm{d}\xi \tag{8}$$

and

$$\mathbf{L}^{-1}_{\xi,\omega} = \int_{-\infty}^{\infty}\int_{-\infty}^{\infty}\mathbf{\Gamma}(x,t)\exp[-\mathrm{i}(\omega t+\xi x)]\mathrm{d}t\mathrm{d}x. \tag{9}$$

Performing the inverse Fourier transform in Eq. (7) and according to the convolution theorem, and the causality condition of the mechanical model, one obtains the column vector of the displacements

$$\begin{aligned}\mathbf{w}(x,t) &= \frac{1}{4\pi^2}\int_{-\infty}^{\infty}\int_{-\infty}^{\infty}\mathbf{L}^{-1}_{\xi,\omega}\mathbf{Q}(\xi,\omega)\exp[\mathrm{i}(\omega t+\xi x)]\mathrm{d}\xi\mathrm{d}\omega \\ &= \int_0^t\int_{-\infty}^{\infty}\mathbf{\Gamma}(x-x',t-t')\{\mathbf{q}(x',t')\}\mathrm{d}x'\mathrm{d}t'.\end{aligned} \tag{10}$$

The matrix $\mathbf{\Gamma}(x\text{-}x',t\text{-}t')$ represents the solution of the equation

$$\mathbf{L}_{x,t}\mathbf{\Gamma}(x-x',t-t') = \delta(x-x')\delta(t-t')\mathbf{E}_2 \tag{11}$$

where $\mathbf{E}_2$ stands for the 2×2 unit matrix. Indeed, performing the Fourier transform, one obtains the necessary equality

$$\exp[-\mathrm{i}(\omega t'+\xi x')]\mathbf{L}_{\xi,\omega}\mathbf{L}_{\xi,\omega}^{-1} = \exp[-\mathrm{i}(\omega t'+\xi x')]\mathbf{E}_2 \tag{12}$$

because

$$\int_{-\infty}^{\infty}\int_{-\infty}^{\infty}\mathbf{\Gamma}(x-x',t-t')\exp[-\mathrm{i}(\omega t+\xi x)]\mathrm{d}t\mathrm{d}x =$$

$$\int_{-\infty}^{\infty}\int_{-\infty}^{\infty}\mathbf{\Gamma}(u,v)\exp\{-\mathrm{i}[\omega(u+t')+\xi(v+x')]\}\mathrm{d}u\mathrm{d}v = \exp[-\mathrm{i}(\omega t'+\xi x')]\mathbf{L}_{\xi,\omega}^{-1}$$

and

$$\int_{-\infty}^{\infty}\int_{-\infty}^{\infty}\delta(x-x')\delta(t-t')\exp[-\mathrm{i}(\omega t+\xi x)]\mathrm{d}t\mathrm{d}x = \exp[-\mathrm{i}(\omega t'+\xi x')]\,.$$

The matrix $\mathbf{\Gamma}(x\text{-}x',t\text{-}t')$ is termed as *the Green's matrix* associated to the operator $\mathbf{L}_{x,t}$ through the equation (11) and will be write as $\mathbf{\Gamma}(x,x',t\text{-}t')$. Taking into account the particular column vector $\mathbf{q}(x,t)$, one needs only the first column of the matrix $\mathbf{\Gamma}(x,x',t\text{-}t')$, denoted as $\mathbf{g}(x,x',t\text{-}t') = [g_1(x,x',t\text{-}t') \quad g_2(x,x',t\text{-}t')]^{\mathrm{T}}$, which contains the time-domain Green's functions of the rail and the slab. These functions describe the responses of the rail and the slab, in the section x at the moment $t\text{-}t'$, if an impulse force occurred at the moment t' in the section x' along the rail. Therefore, $\mathbf{g}(x,x',t\text{-}t')$ will be called the column vector of *the time-domain Green's functions of the track*.

In these circumstances, the column vector of the displacements can be calculated as follows

$$\mathbf{w}(x,t) = \int_0^t\int_{-\infty}^{\infty}\mathbf{g}(x,x',t-t')Q(t')\delta(x'-Vt')\mathrm{d}x'\mathrm{d}t' = \int_0^t\mathbf{g}(x,Vt',t-t')Q(t')\mathrm{d}t'\,. \tag{13}$$

From Eq. (11), it follows that the column vector $\mathbf{g}(x,x',t\text{-}t')$ satisfies the equation (5). □

One can observe that the column vector of the time-domain Green's functions of the rail and the slab are attenuated in space and time-domains:

$$\lim_{|x-x'|\to\infty}\mathbf{g}(x,x',t-\tau) = \lim_{t-\tau\to\infty}\mathbf{g}(x,x',t-\tau) = 0\,. \tag{14}$$

Using the Fourier transform, the column vector $\mathbf{G}(x,x',\omega)=[G_1(x,x',\omega)\ G_2(x,x',\omega)]^{\mathrm{T}}$ can be associated to the column vector of the time-domain Green's functions

$$\mathbf{G}(x,x',\omega) = \int_{-\infty}^{\infty}\{\mathbf{g}(x,x',t)\}\exp(-\mathrm{i}\omega t)\mathrm{d}t\,. \tag{15}$$

The components of the column vector $\{\mathbf{G}(x,x',\omega)\}$ are the frequency-domain Green's functions of the rail and the slab. These functions, termed *the receptances*, represent the response of the rail and the slab in the section x, provoked by a unitary harmonic impulse by an angular frequency ω, occurring in the section x' of the rail. Next, the column vector $\{\mathbf{G}(x,x',\omega)\}$ is called *the column vector of the frequency-domain Green's functions of the track*.

Theorem 2. *The column vector of the frequency-domain Green's functions* $\mathbf{G}(x,x',\omega)$ *has the following properties*:

a) *it verifies the equation*

$$\mathbf{L}_{x,\omega}\mathbf{G}(x,x',\omega)=\delta(x-x')\begin{bmatrix}1 & 0\end{bmatrix}^{\mathrm{T}}, \tag{16}$$

b) *it verifies the equality*

$$\lim_{|x-x'|\to\infty}\mathbf{G}(x,x',\omega)=\lim_{\omega\to\pm\infty}\mathbf{G}(x,x',\omega)=0 \tag{17}$$

c) *it has the form*

$$\mathbf{G}(x,x',\omega)=\int_{-\infty}^{\infty}G_D(x,x_0,\omega)\mathbf{L}^{*}_{x,\omega}\begin{bmatrix}\delta(x_0-x') & 0\end{bmatrix}^{\mathrm{T}}\mathrm{d}x_0, \tag{18}$$

where $\mathbf{L}_{x,\omega}$ *stands for the Fourier transform of the matrix operator* $\mathbf{L}_{x,t}$, $\mathbf{L}_{x,\omega}$ *is the adjoint matrix of the matrix* $\mathbf{L}_{x,\omega}$ *and the function* $G_D(x,x',\omega)$ *remains to be specified later*.

Proof. The first two conditions result by applying the Fourier transform to the equation (5) and the limits (14). In order to arrive to the form (18), Eq. (16) is modified by applying the adjoint matrix operator $\mathbf{L}^{*}_{x,\omega}$,

$$\mathrm{diag}(D,D)\{\mathbf{G}(x,x',\omega)\}=\mathbf{L}^{*}_{x,\omega}\begin{bmatrix}\delta(x-x') & 0\end{bmatrix}^{\mathrm{T}}, \tag{19}$$

where the differential operator

$$D=a_0\frac{\mathrm{d}^8}{\mathrm{d}x^8}+a_4\frac{\mathrm{d}^4}{\mathrm{d}x^4}+a_8 \tag{20}$$

has the complex coefficients a_0, a_4 and a_8 depending on the track's parameters and the angular frequency

$$\begin{gathered}a_0=EI_1EI_2,\\ a_4=EI_1\left[k_1+k_2-\omega^2m_2+\mathrm{i}\omega(c_1+c_2)\right]+EI_2(k_1-\omega^2m_1+\mathrm{i}\omega c_1),\\ a_8=\omega^4m_1m_2-\mathrm{i}\omega^3\left[m_1(c_1+c_2)+m_2c_1\right]-\omega^2\left[m_1(k_1+k_2)+m_2k_1+c_1c_2\right]+\\ +\mathrm{i}\omega(k_1c_2+k_2c_1)+k_1k_2.\end{gathered} \tag{21}$$

Finally, the column vector of the frequency-domain Green's functions results from Eqs. (19) and takes the form (18), where $G_D(x,x',\omega)$ is the Green's function of the operator D. □

To perform the integral from Eq. (18), the Green's function of the operator D is required. In fact, this function verifies the equation

$$DG_D(x,x',\omega)=\delta(x-x') \tag{22}$$

and the boundary conditions

$$\lim_{x\to\pm\infty}G_D(x,x',\omega)=0 \tag{23}$$

due to the damping of the track.

This kind of equation is usually solved by applying the Fourier transform from the space-domain to the wave-number domain and then, by using the inverse

Fourier transform via the contour integration given by the theory of the functions of complex variables [2].

In this paper, a different solution is considered and the Green's function of the D operator is obtained using its outstanding features [13]. The ODE $Dy=0$ has the following solutions

$$y_i(x) = A_i \exp(\lambda_i x) \text{ with } i = 1 \div 8, \tag{24}$$

where $\lambda_i = \lambda_i(\omega)$ are eigenvalues of the operator D. It can be seen that if λ_i is one solution of the characteristic equation, then $-\lambda_i$ and $\pm i\lambda_i$ are solutions as well. Practically, each quadrant contains two solutions of the D operator characteristic equation.

In fact, λ_i describes the bending wave, which propagates through the track structure. The bending wave is a propagating one when λ_i is an imaginary quantity. This wave propagates from the left to the right when Im $\lambda_i > 0$, and vice versa when Im $\lambda_i < 0$. The bending wave attenuates when λ_i is a complex number. According to the boundary conditions, the attenuated wave decreases with distance (Re$\lambda_i > 0$ for $x \to -\infty$ and Re$\lambda_i < 0$ for $x \to \infty$). Finally, the bending wave is an evanescent one when λ_i is a real quantity. In addition, the evanescent wave has to propagate following the same rule as the attenuated one, according to the boundary conditions.

According to previous considerations, the Green's function of the operator D has the forms

$$\begin{aligned} G_D^-(x,x_0,\omega) &= \sum_{i=1}^{4} A_i(x_0)\exp(\lambda_i x) \text{ for } -\infty < x < x_0, \\ G_D^+(x,x_0,\omega) &= \sum_{i=5}^{8} A_i(x_0)\exp(\lambda_i x) \text{ for } x_0 < x < \infty, \end{aligned} \tag{25}$$

with Re$\lambda_i > 0$ for $i = 1 \div 4$ and Re$\lambda_i < 0$ for $i = 5 \div 8$.

On the other hand, the Green function is continuous at $x = x_0$ and its first 6 derivates are continuous as well

$$G_D^-(x_0,x_0,\omega) = G_D^+(x_0,x_0,\omega), \ \frac{\mathrm{d}^n G_D^-}{\mathrm{d}x^n}(x_0,x_0,\omega) = \frac{\mathrm{d}^n G_D^+}{\mathrm{d}x^n}(x_0,x_0,\omega), \ n = 1 \div 6. \tag{26}$$

Further on, the 7th derivative of the Green's function has a discontinuity at $x=x_0$

$$\frac{\mathrm{d}^7 G_D^+}{\mathrm{d}x^7}(x_0+0,x_0,\omega) - \frac{\mathrm{d}^7 G_D^-}{\mathrm{d}x^7}(x_0-0,x_0,\omega) = \frac{1}{a_0}. \tag{27}$$

All these conditions lead to the next matrix equation

$$\begin{bmatrix} 1 & 1 & ... & 1 \\ \lambda_1 & \lambda_2 & ... & \lambda_8 \\ ... & ... & ... & ... \\ \lambda_1^7 & \lambda_2^7 & ... & \lambda_8^7 \end{bmatrix} \begin{bmatrix} X_1 \\ X_2 \\ ... \\ X_8 \end{bmatrix} = \begin{bmatrix} 0 \\ 0 \\ ... \\ -a_0^{-1} \end{bmatrix} \tag{28}$$

where $X_i = A_i(x_0)\exp(\lambda_i x_0)$ for $i = 1 \div 4$ and $X_i = -A_i(x_0)\exp(\lambda_i x_0)$ for $i = 5 \div 8$. Obviously, the matrix from Eq. (28) has the Vandermonde determinant and in fact, all Cramer's determinants are Vandermonde determinants, as well.

Eq. (28) has the following solution

$$X_i = \frac{1}{a_0 \prod_{k \neq i} (\lambda_k - \lambda_i)}, \text{ with } i, k = 1 \div 8 \tag{29}$$

and finally, the Green's function of the D operator is obtained

$$G_D^-(x, x_0, \omega) = \frac{1}{a_0} \sum_{i=1}^{4} \frac{\exp[\lambda_i (x - x_0)]}{\prod_{k \neq i} (\lambda_k - \lambda_i)} \text{ for } -\infty < x < x_0,$$

$$G_D^+(x, x_0, \omega) = -\frac{1}{a_0} \sum_{i=5}^{8} \frac{\exp[\lambda_i (x - x_0)]}{\prod_{k \neq i} (\lambda_k - \lambda_i)} \text{ for } x_0 < x < \infty. \tag{30}$$

Introducing the Green's function of the D operator from Eq. (30) in Eq. (18) and performing the integral, one obtains

$$\begin{bmatrix} G_1(x, x', \omega) \\ G_2(x, x', \omega) \end{bmatrix} = \begin{bmatrix} K \sum_{i=1}^{2} (-1)^{i-1} (p\lambda_i^4 + r) \dfrac{\exp(-\lambda_i |x - x'|) - \mathrm{i} \exp(\mathrm{i}\lambda_i |x - x'|)}{\lambda_i^3} \\ sK \sum_{i=1}^{2} (-1)^{i-1} \dfrac{\exp(-\lambda_i |x - x'|) - \mathrm{i} \exp(\mathrm{i}\lambda_i |x - x'|)}{\lambda_i^3} \end{bmatrix}, \tag{31}$$

where $\lambda_{1,2}$ are contained in the first quadrant and

$K^{-1} = 4EI_1EI_2(\lambda_2^4 - \lambda_1^4)$, $p = EI_2$, $r = k_1 + k_2 - \omega^2 m_2 + \mathrm{i}\omega(c_1 + c_2)$, $s = k_1 + \mathrm{i}\omega c_1$.

It is important to emphasize that the time-domain Green's functions of the rail and the slab will be computed from the corresponding frequency-domain Green's functions.

Performing the inverse Fourier transform applied to the frequency-domain Green's functions, it follows that the time-domain Green's functions for the track are

$$\begin{aligned} \mathbf{g}(x, x', t - \tau) &= \frac{1}{2\pi} \int_{-\infty}^{\infty} \mathbf{G}(x, x', \omega) \exp[\mathrm{i}\omega(t - \tau)] \mathrm{d}\omega \\ &= \frac{2}{\pi} \int_0^{\infty} \mathrm{Re}\mathbf{G}(x, x', \omega) \cos[\omega(t - \tau)] \mathrm{d}\omega. \end{aligned} \tag{32}$$

The last expression resides from the causal character of the track model and it is used effectively for the computation. More precisely, the time-domain

Green's functions are calculated by numerical integration with the help of the cubic spline functions invoking the following properties.

According to the attenuation in time-domain, there is a certain T for which the norm of the Green's functions is "concentrated" in the [0, T] interval. Therefore, the column vector of the displacements at loading section ($x = Vt$) results as

$$\mathbf{w}(Vt,t) = \int_0^t \mathbf{g}(Vt, V\tau, t-\tau)Q(\tau)\mathrm{d}\tau \text{ , for } 0 \le t < T \tag{33}$$

$$\mathbf{w}(Vt,t) \cong \int_{t-T}^t \mathbf{g}(Vt, V\tau, t-\tau)Q(\tau)\mathrm{d}\tau \text{ , for } t \ge T. \tag{34}$$

It may be observed that for any contact section point $x = Vt$, there is a corresponding column vector of the Green's functions $\mathbf{g}(Vt, V\tau, t\text{-}\tau)$ which depends on $0 \le \tau \le t$ and it is calculated from $\mathbf{g}(x, x', t\text{-}\tau)$. For the particular case when $t > T$, only the history for $\tau \in [t - T, t]$ is necessary, according to the attenuation in time-domain. Moreover, all contact points $x = Vt$ with $t > T$ have the same sequence of column vector of the time-domain Green's functions because the track has the homogeneous structure.

From the numerical integration point of view, there are two steps to follow: the first refers to $0 \le t < T$ - the 'transitory' period of numeric integration, while the second assumes $T \le t$, which means the 'stationary' period of numerical integration. As results, the numerical simulation length has to be higher than the transitory T period.

When is used the small time-steps method on short Δt time intervals in order to integrate the equations of motion, the time-domain Green's functions will be calculated in $N = T/\Delta t + 1$ and all the obtained values may be encapsulated in the so-called *track's Green matrix* which depends on the speed value V. This matrix includes the required values for the transitory period of numerical integration.

More specific, a time partition - $t_0, t_1, \ldots t_n$ with t_0=0, t_n=t and Δt=t_i - $t_{i\text{-}1}$ where $i = 1 \div n$ - should be considered. The track's Green matrix has the form

$$\mathbf{g}_t = \left[\mathbf{g}^1 \ \mathbf{g}^2 \ \ldots \mathbf{g}^i \ \ldots \mathbf{g}^N\right], \tag{36}$$

where $\mathbf{g}^i$=$\mathbf{g}(Vt_N, Vt_i, t_N\text{-}t_i)$.

The column vector of the displacements at the loading section may be defined as

$$\mathbf{w}(Vt_n, t_n) = \sum_{i=1}^{n} \int_{t_{i-1}}^{t_i} \mathbf{g}(Vt_n, V\tau, t_n - \tau)Q(\tau)\mathrm{d}\tau \,. \tag{37}$$

Assuming that in the time interval [$t_{i\text{-}1}$, t_i], the Green functions and the normal contact force $Q(\tau)$ have a linear variation, the previous integrations may be performed

$$\mathbf{w}(Vt_n, t_n) = \Delta t \sum_{i=1}^{n} \left[\frac{\mathbf{g}^{i-1} Q_i + \mathbf{g}^i Q_{i-1}}{2} + \frac{(\mathbf{g}^i - \mathbf{g}^{i-1})(Q_i - Q_{i-1})}{3} \right], \tag{38}$$

where $Q_i = Q(t_i)$ and $\mathbf{g}^i$ is taken from the track's Green matrix. For $t_n > T$, the rail and slab displacements will be calculated by summing N terms only, according to Eq. (34). For the column vector of the displacements at a particular section of the track, the similar formulae have to be computed.

3. Numerical results

Further on, both frequency and time-domain numerical analysis of a particular slab track under a moving load is presented.

Physical parameters of the track model used in these computations are as follows: $m_1 = 60$ kg/m, $EI_1 = 6.42$ MNm^2, $m_2 = 1750$ kg/m, $EI_2 = 274$ MNm^2, $k_1 = 52$ MN/m^2, $c_1 = 7$ kNs/m^2, $k_2 = 60$ MN/m^2 and $c_2 = 40$ kNs/m^2.

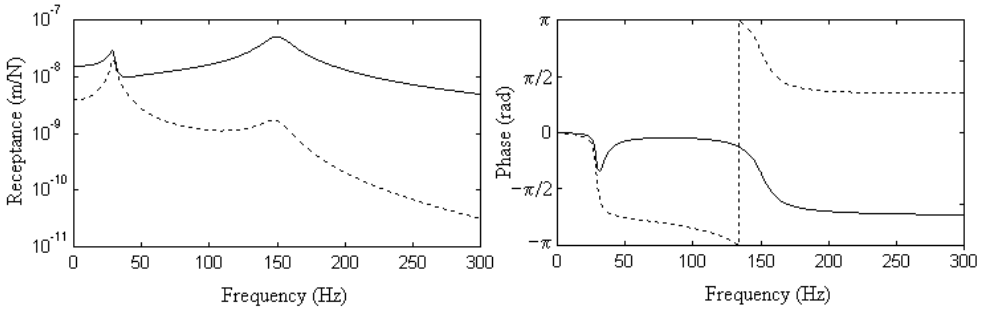

Figure 2. Green's functions of the slab track for the frequnecy-domain analysis: ——, rail; ----, slab.

Fig. 2 presents the frequency-domain Green's functions of the track, i.e. the rail and slab receptances, which have been computed at the point of a unitary harmonic impulse force. As it can be observed, the track response has two peaks at 29 and 150 Hz because the rail and the slab vibrate as a discrete system with two degrees of freedom. At the first resonance frequency, the rail and the slab are in phase and then, they vibrate in anti-phase. The first peak belongs to the slab resonance, and the second one is the effect of the rail's resonance. The two frequencies of resonance may be approximately calculated using the formula from the single-degree-of freedom system consisting of an equivalent mass and a spring with equivalent stiffness

$$f_{1,2} = \frac{1}{2\pi} \sqrt{\frac{k_{1,2}}{m_{1,2}}} \, .$$

The rail receptance is significantly higher than the slab receptance due to its low inertia and the elasticity of the rail-pad. The diagram of the track's receptances is similar with the results from the preceding related researches [3, 5].

Fig. 3 shows the influence of the speed of the moving harmonic load on the receptance of the rail. In order to calculate the receptance of the rail due to moving harmonic load, the equations of motion have been solved introducing the moving frame and then, following the same method. It can be seen that by increasing the speed of moving harmonic load, the resonance frequencies of the track decrease. In addition, the receptance of the rail lows around resonance frequencies due to the speed of the harmonic excitation.

The Green's functions of the track for the time-domain analysis may be calculated by the numerical integration of Eq. (31) from 0 to 5 kHz with the step integration of 2 Hz.

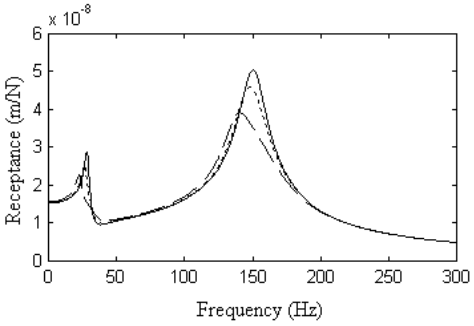

Figure 3. Receptance of the rail at different speeds: ——, 0 m/s; ----, 60 m/s; — —, 120 m/s.

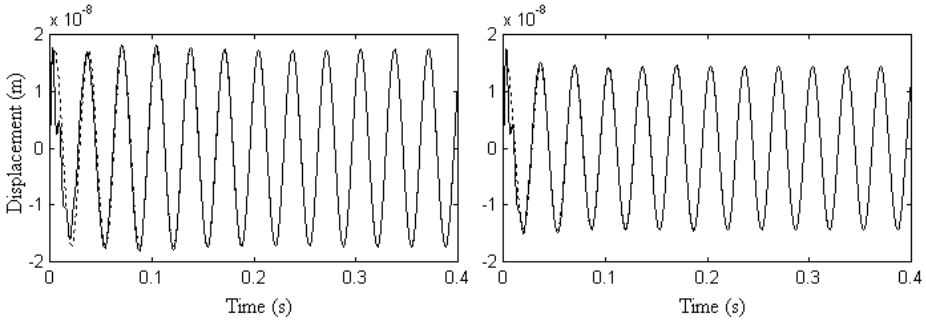

Figure 4. Displacement of the loading point (a) at 60 m/s and (b) at 120 m/s: ——, the numerical solution; ----, the steady-state behaviour.

Fig. 4 presents the displacement of the loading point for the frequency of the unitary harmonic load of 30 Hz and for two values of the speed, 60 and 120 m/s. To this end, Eq. (38) has been used. The results of the steady-state behaviour

given by the analytical solution are presented as well for comparison. It may observe the transitory behaviour in the case of the numerical solution. The two solutions are very similar. Indeed, the difference between the amplitudes obtained by the two methods is 0.385 % at 60 m/s and 0.102% at 120 m/s.

Fig. 5 presents the displacement of the fixing point belonging to the section of the rail situated at 24 m from the frame, when a unitary harmonic load with the frequency of 30 Hz travels along the rail at 60 m/s. In this case, Eq. (6) is applied. The simulation of the steady-state behaviour is shown using an analytical method. Once again, the results from the numerical and analytical method are matched. The relative error between the results given by the two methods is 0.283 % for the displacement obtained at t = 0,4 s, when the harmonic load passes over the fixing point. It has underline that the fixing point vibrates more intense in the trace of the moving load.

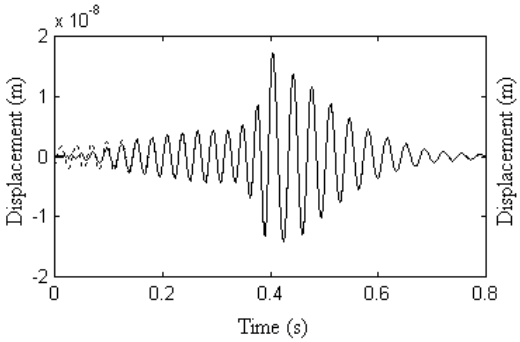

Figure 5. Displacement of the fixing point: —, numerical solution, ----, steady-state behaviour.

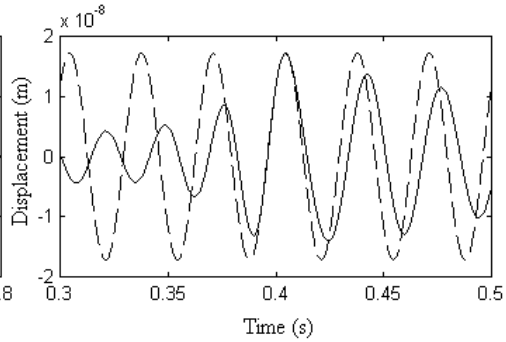

Figure 6. Displacement of the rail: —, fixing point, — —, loading point.

Fig. 6 displays the displacement of the loading point and the displacement of the fixed point previously presented. The displacement of the loading point and the displacement of the fixed point have the same value only when the moving load passes over the section of the fixed point. At 30 Hz, the bending wave of the rail is a propagating one that propagates from the moving load to the fixing point. Due to this, the history of the fixed point is later than the loading point's except in the joining moment. For instance, one can observe that all peaks of the fixed point are later than the corresponding ones of the loading point. Consequently, the fixed point has a frequency higher than the loading point's one before the joining and then, after joining, this trend reverses. In other words, this is the Doppler effect.

4. Conclusions

The response of the slab track under a moving load has been studied, considering the model of an infinite homogenous structure consisting of two Euler-Bernoulli beams continuously supported by elastic layers.

To this aim, the method of Green's functions has been applied following the numerical approach. The high accuracy of the presented method has been verified. The proposed method is important because allows us to simulate the wheel/rail interaction under nonlinear conditions.

The structure response due to stationary and moving harmonic loads has been investigated for both frequency and time domains.

Acknowledgements

This paper has been partially supported by the University Politehnica of Bucharest. The author would like to express his sincere thanks to Prof. Dr. Constantin Udrişte, University Politehnica of Bucharest, for kind encouragement and support.

R E F E R E N C E S

[1]. *J. Bitzenbauer, J. Dinkel*, Dynamic interaction between a moving vehicle and an infinite structure excited by irregularities – Fourier transforms solution, Archive of Applied Mechanics **73**, 131-141, 2003.

[2]. *M. F. M. Hussein, H. E. M. Hunt*, Modelling of floating-slab tracks with continuous slabs under oscillating moving loads, Journal of Sound and Vibration, **297**, 37-54, 2006.

[3]. *M. Shamalta, A. V. Metrikine*, Analytical study of the dynamic response of an embedded railway track to a moving load, Archive of Applied Mechanics **73**, 131-146, 2003.

[4]. Knothe, K., Grassie, S., Modelling of railway track and vehicle/track interaction at high frequencies, Vehicle System Dynamics **22**, 209-263, 1993.

[5]. *K. Popp, H. Kruse, I. Kaiser*, Vehicle-Track Dynamics in the Mid-Frequency Range, Vehicle System Dynamics, **31**, 423-464, 1999.

[6]. L. Fryba, History of Winkler foundation, Vehicle System Dynamics Supplement **24,** 7-12, 1995.

[7]. *T. X. Wu, D. J. Thompson*, Theoretical Investigation of Wheel/Rail Nonlinear Interaction due to Roughness Excitation, Vehicle System Dynamics **34**, 261-281, 2000.

[8]. *T. X. Wu, D. J. Thompson*, A hybrid model for the noise generation due to railway wheel flats, Journal of Sound and Vibration **251**, 115-139, 2002.

[9]. *Tr. Mazilu*, Green's functions for analysis of dynamic response of wheel/rail to vertical excitation, Journal of Sound and Vibration, **306**, 31-58, 2007.

[10]. *Tr. Mazilu*, Wheel/Rail Vibrations (in Romanian), MatrixRom, Bucharest, 2008.

[11]. *Tr. Mazilu*, Analysis of infinite structure response due to moving mass in the presence of irregularities via Green's functions method, Proceedings of Romanian Academy, Series A, vol. **10**, No. 2, 2009.
[12]. *L. Cremer, M. Heckl*, Structure-Borne Sound Structural Vibrations and Sound Radiation at Audio Frequencies, Spinger-Verlag Berlin, Heildelberg, 1973 and 1988.
[13]. *Gh. Mocică*, The Laplace Transform and Operational Methods (in Romanian), UPB, Bucharest, 1993.